Available online at www.sciencedirect.com
SCIENCE DIRECT®
Journal of Molecular Catalysis A: Chemical 233 (2005) 73–81
JOURNAL OF MOLECULAR CATALYSIS A: CHEMICAL
www.elsevier.com/locate/molcata

Iron porphyrins immobilised on silica surface and encapsulated in silica matrix: a comparison of their catalytic activity in hydrocarbon oxidation

Maria Silvia Monsalves Moreira [a], Patrícia R. Martins [a], Rebeca B. Curi [a], Otaciro R. Nascimento [b], Yassuko Iamamoto [a,*]

[a] *Departamento de Química, FFCLRP, Universidade de São Paulo, Av. Bandeirantes 3900, Ribeirão Preto, SP, CEP 14040-901, Brazil*
[b] *Instituto de Física de São Carlos, USP, São Carlos, SP, CEP 13560-250, Brazil*

Received 5 November 2004; received in revised form 27 January 2005; accepted 27 January 2005

Abstract

In this work, different iron porphyrins, either immobilised on silica surface or encapsulated in silica matrix (FePES), have been used as catalyst in hydrocarbon oxidation by PhIO or H_2O_2, and results have been compared. Such study has aimed at understanding the relationship between the catalytic results and the following properties of the catalytic reaction sites: (i) the coordination environment around the central iron, which can change substrate binding; (ii) the nature of the support, since polarity can affect substrate accessibility to the active site; (iii) the FeP nature and the microenvironment it create. We have observed that all systems are able to oxidise (*Z*)-cyclooctene and cyclohexane, and better product yields are obtained with the supported systems. In the case of FePES, high cyclohexanol and epoxide yields are obtained with the electronegatively substituted Im-[FeTFPP]ES. The low yields obtained with the cationic FePES can be explained by the polar environment of the FeP active site, which hinders the oxygen rebound mechanism necessary for the hydroxylation of the inert cyclohexane. As for the supported systems, commercial silica leads to high epoxidation and hydroxylation yields, showing that cationic iron porphyrins are efficient catalysts even when immobilised on a simple support. The use of the clean oxidant H_2O_2 for olefin epoxidation in cases of the 2- and 4-*N*-methyl-pyridyl substituted FePs in heterogeneous systems is reported for the first time in this paper, and the results are comparable with literature data on electron-deficient FePs in homogeneous systems. The best catalyst is $[Fe(TF4TMAPP)]^{5+}$ on the SiSH and SiO_2 supports rendering 80% and 86% epoxide yields with H_2O_2, respectively. All materials have been characterised by BET analysis, UV–vis and EPR spectroscopies.

Keywords: Iron porphyrin; Encapsulated; Supported on silica; Catalyst; H_2O_2

1. Introduction

Cytochrome P450s are a class of heme-containing monooxygenases that transfer an oxygen atom from molecular oxygen to a wide range of organic substrates [1]. In an attempt to mimic the reactivity of heme proteins, many researchers have used metalloporphyrins to catalyse a variety of hydrocarbon oxidations with various oxygen donors [2,3]. These include iodosylbenzenes, peroxyacids, hypochlorite, chlorite, hydroperoxides, N-oxides, hydrogen peroxide, monoperoxyphthalate and potassium monopersulfate [4]. In particular, the reactions of metalloporphyrins with hydrogen peroxide have attracted much attention in the iron porphyrin (FeP) oxidation chemistry, since H_2O_2 is a biologically important and environmentally clean oxidant, leading to the formation of only a water molecule as side-product [4,5].

The growing development in the search for catalysts that are stable in the reaction media and promote selective hydrocarbon oxidations with high turnovers has been a challenge in biomimetic chemistry. However, a problem associated with metalloporphyrins catalysed oxidation is catalyst oxidative self-destruction in the oxidizing media [2,6]. One approach

* Corresponding author. Tel.: +55 16 602 3782; fax: +55 16 633 8151.
E-mail address: iamamoto@usp.br (Y. Iamamoto).

1381-1169/$ – see front matter © 2005 Elsevier B.V. All rights reserved.
doi:10.1016/j.molcata.2005.01.045

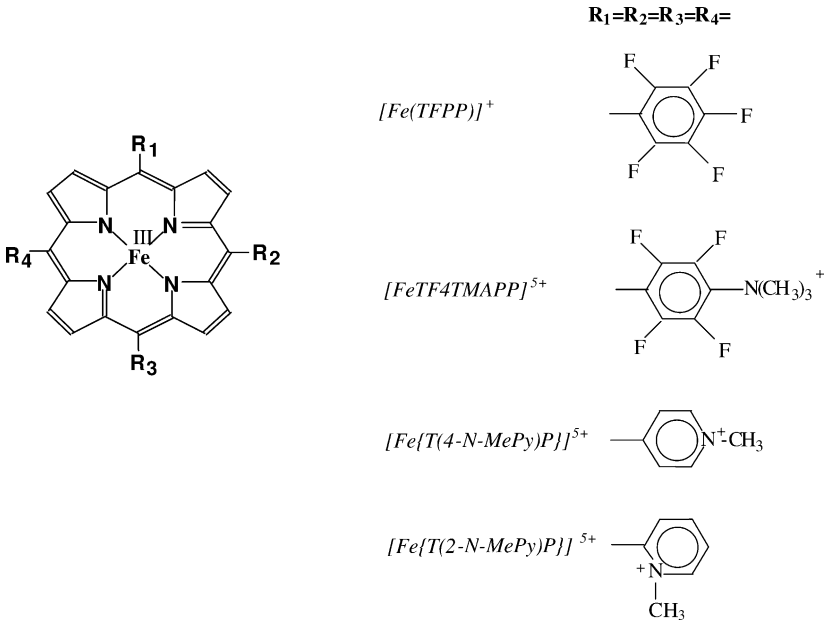

Fig. 1. FePs used in this work.

to solve this problem is the use of electron-withdrawing substituents on the porphyrin periphery, especially halogenated and perhalogenated phenyl porphyrins, which produces robust and resistant catalysts [7–10]. Another solution to promote the stability of metalloporphyrin catalysts is to immobilise them on a solid matrix. This can provide added benefits arising from steric and electronic effects of the support, which are in some respects analogous to the influence of the polypeptide chain in hemeproteins [11]. In general, immobilisation methods include physical entrapment, covalent binding and surface adsorption.

Our group has devoted efforts to the study of the catalytic activity of various systems anchored on silica surface [12,13] and encapsulated in the silica matrix through the sol–gel process [14]. In the present work, we describe (*Z*)-cyclooctene epoxidation and cyclohexane hydroxylation by iodosylbenzene in the presence of different iron porphyrins (Fig. 1) anchored on silica surface (Fig. 2) or encapsulated in the silica matrix through the sol–gel process. In recent studies, many relevant results for olefin epoxidation [5] and alkane hydroxylation [15] in homogeneous systems have been reported, using H_2O_2 as oxidant. However, few results have been reported with supported systems. In this paper, we have studied (*Z*)-cyclooctene epoxidation with H_2O_2 catalysed by different iron porphyrins in heterogeneous systems. We have analysed results and discussed the probable mechanisms involved in the reactions.

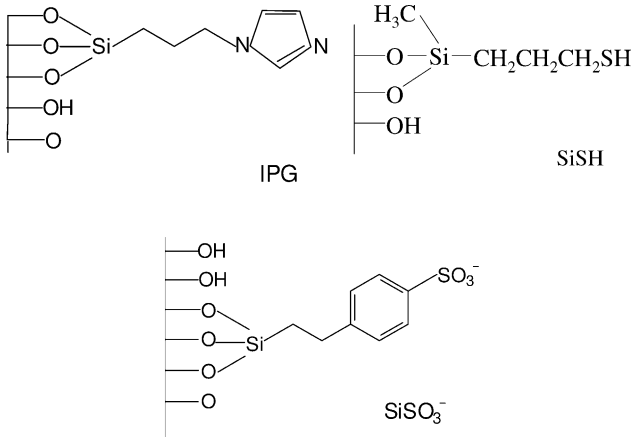

Fig. 2. Supports used to anchor FePs.

2. Experimental

2.1. Materials

N,*N*′-dimethylformamide (DMF, Merck) was placed over KOH pellets for 24 h, refluxed for 12 h, distilled and stored in a dark bottle with 0.4 nm molecular sieves. 1,2-Dichloroethane (DCE, Merck) was distilled and stored over 0.4 nm molecular sieves. (*Z*)-cyclooctene was purified by column chromatography on basic alumina prior to use. Iodosylbenzene (PhIO) was prepared through the hydrolysis of iodobenzenediacetate [16], and it was stored in a freezer; its purity was measured by iodometric assay. Hydrogen peroxide (30%, w/v) was stored at 5 °C and titrated periodically. Tetraethilorthosilicate (TEOS, Aldrich), ethanol (EtOH, Synth), dichloromethane (DCM, Synth), pyridine (Merck), imidazole (Sigma), 4-phenylimidazole (Acros) and carbon tetrachloride (CCl_4, Carlo Erba) were used as received.

2.2. Iron porphyrins

2.2.1. Tetrakis(2,3,4,5,6-pentafluorophenyl)porphyrin ([Fe(TFPP)]$^{+}$)

The synthesis of $TFPPH_2$ was carried out according to Lindsey's method [17], as previously described [18]. The obtained $TFPPH_2$ was characterised by UV–vis spectroscopy and ^{1}H NMR, which confirmed the structure and the purity of the porphyrin [19]. Iron insertion into $TFPPH_2$ was performade as described by Kadish et al. [20].

2.2.2. Iron(III) meso-tetrakis(2,3,5,6-tetrafluoro-N,N,N,-trimethyl-4-anilinium)porphyrin ([FeTF4TMAPP]$^{5+}$) and iron(III) meso-tetrakis(2-N-methylpyridyl)porphyrin ([Fe{T(2-N-MePy)P}]$^{5+}$)

These FePs were purchased from Midcentury and used as received.

2.2.3. Iron(III) meso-tetrakis(4-N-methylpyridyl)porphyrin ([Fe{T(4-N-MePy)P}]$^{5+}$)

This FeP was obtained from [T(4-*N*-MePy)P]$^{4+}$ (purchased from Midcentury). Iron was inserted into [T(4-*N*-MePy)P]$^{4+}$ with $FeCl_2{\cdot}4H_2O$, by the method described by Kachadourian et al. [21].

2.3. Solid supports

IPG and $SiSO_3^-$ were obtained and characterised as recently reported [22]. SiSH was prepared by heating a suspension of silica gel with (3-mercapto-propyl)methyldimethoxysilane, according to the method of Basolo and coworkers [23], and the resulting material was dried under vacuum at 100 °C, for 8 h. Elemental analysis: C = 1.2%; H = 1.0%; S = 0.9%, which corresponds to 2.5×10^{-4} mol of methyldimethoxymercaptopropyl/g of SiSH. SiO_2 was used as received (purchased from Carlo Erba).

2.4. Preparation of supported iron porphyrins

Supported iron porphyrins were achieved by stirring the respective FeP solution in ACN or MeOH with a suspension of the support for about 30 min. The amount of complex bound to the solid matrix was 7.5×10^{-6} mol of FeP/g of support. The resulting catalysts were washed with ACN or MeOH in a Soxhlet extractor overnight to remove unbound and weakly bound FeP. The solids were dried for 5 h, at 100 °C. The loading was quantified by measuring the amount of unloaded FeP in the combined reaction solvent and washings by UV–vis spectroscopy.

2.5. Preparation of entrapped iron porphyrin (FePES)

Initially, the silica sol was prepared by stirring 20 ml of ethanol (EtOH), 3.0 ml of tetraethylorthosilicate (TEOS) and 0.5 ml of water for 2 h [24]. The FeP (3.0 mg) (3.30×10^{-6} mol) and 1×10^{-4} mol of the template (imidazole or 4-phenylimidazole) were then added. The resulting solution was stirred at 25 °C until the xerogel was formed. The obtained xerogel was allowed to stand under cover at 90 °C. The resulting solid was ground and washed with various solvents, in the following order: acetone, methanol, water, methanol, acetone and dichloromethane. The solid was washed in a Soxhlet extractor with MeOH, for 24 h. The amount of iron(III)porphyrin leached from the silica material was quantified by measuring the UV–vis absorbance.

2.6. UV–vis spectra

Electronic spectra (UV–vis) were recorded in a UV–vis spectrophotometer (Hewlett Packard 8453 Diode Array). For both supported and encapsulated iron porphyrins, spectra were recorded in a 2 mm-path-length quartz cell, with the solid catalyst in a suspension in CCl_4. The "blank" had been previously recorded and consisted of a support/CCl_4 suspension.

2.7. EPR spectra

Electron paramagnetic resonance (EPR) spectra of the solids were performed using a commercial X-band spectrometer (Bruker Elexsys line E-580) equipped with a standard rectangular cavity. The temperature ~4 K was controlled by using a low temperature accessory (Helitran Oxford Systems). The materials EPR spectra were recorded after adding 0.030–0.050 g of the dry material to an EPR quartz tube.

2.8. Surface area

Specific surface area was determined by the BET method from nitrogen adsorption data, using a physical adsorption analyzer (Micrometrics Accsorb 2100 E) [25].

2.9. Titration of iron porphyrin with nitrogen base

A 1–20 μl aliquots of pyridine or nitrogen base solution (imidazole or 4-phenylimidazole, 0.1 mol l^{-1}) were added to a 2.0 mm-path-length quartz cell containing 200 μl of an FeP solution in DCE (2×10^{-4} mol l^{-1}). The resulting spectra were recorded on a UV–vis spectrophotometers, HP 8453 Diode Array.

2.10. Product analysis by gas chromatography

Gas chromatographic analyses were performed on a gas chromatograph (Hewlett Packard HP 6890 Series GC System), coupled to a flame ionization detector, using a capillary column (HP-INNOWAX, cross-linked poly(ethylene glycol), length 30 m; i.d. 0.25 mm, film thickness 0.25 μm) and nitrogen as the carrier gas.

2.11. Procedure for catalytic oxidations

All substrates were checked by gas chromatography prior to use, to ensure that they were free from oxidation products. Reactions were performed in a 4 ml vial with a teflon-coated silicone septum and stirred at room temperature. In a standard reaction, 2.5×10^{-7} mol of FeP, 200 μl of substrate ((*Z*)-cyclooctene or cyclohexane) and 2 or 5 μl of bromobenzene (internal standard) were mixed in 800 μl of solvent (DCE in the case of PhIO as oxidant, and DCM:ACN (1:1) in the case of H_2O_2 as oxidant). Yields based on the added oxidant were determined by removing aliquots of the reaction mixture and analysing them by gas chromatography.

3. Results and discussion

3.1. Preparation and characterization of anchored iron porphyrins

The anchored FePs were prepared by stirring a suspension of the support (IPG, $SiSO_3^-$, SiO_2 or SiSH) in a solution of FeP in ACN or MeOH. These materials were subsequently washed in a Soxhlet extractor with ACN or MeOH overnight, to remove unbound and weakly bound FeP. This ensured that the FeP would not leach from the support throughout the oxidation reactions carried out in DCE (in the case of PhIO as oxidant) or DCM:ACN (1:1) (in the case of H_2O_2 as oxidant) at 25 °C, making sure that the yields attained with the heterogeneous catalysts would only be due to the supported FeP catalytic activity. The washed catalysts were isolated by filtration and dried for 5 h, at 100 °C.

The supports IPG, $SiSO_3^-$ and SiSH were selected because they are oxidatively stable under the reaction conditions and allow the study of the catalytic activity of cationic FeP anchored to solid surfaces in two different ways: (i) through electrostatic interaction between the cationic groups of the FeP and counterionic groups on the surface of $SiSO_3^-$, and (ii) through coordinating groups on the surface of IPG and SiSH. Another reason for using charged supports was that it was expected to give rise to stronger FeP-support binding than IPG or SiSH [26,27].

The electronic spectra of the anchored catalysts confirmed the presence of FeP on the supports, being a qualitative method of characterisation. Despite the difficulty in obtaining information at a molecular level inherent to this technique [22,28], some qualitative information could be obtained: the spectrum of [Fe(TF4TMAPP)]$(PF_6)_5$ in ACN displays a band at 334 nm, and Soret peak at 412 nm (Fig. 3A). After the addition of (3-mercapto-propyl)-methyldimethoxysilane (FeP/ligand ratio = 1:37), the band at 334 nm disappears and the Soret peak shifts to 418 nm (Fig. 3B), indicating that when this FeP coordinates to the –SH group, it does not display a band at 334 nm. However, the solid catalyst [Fe(TF4TMAPP)]-SiSH does display a band at 334 nm, a pattern which is very similar to that obtained with the

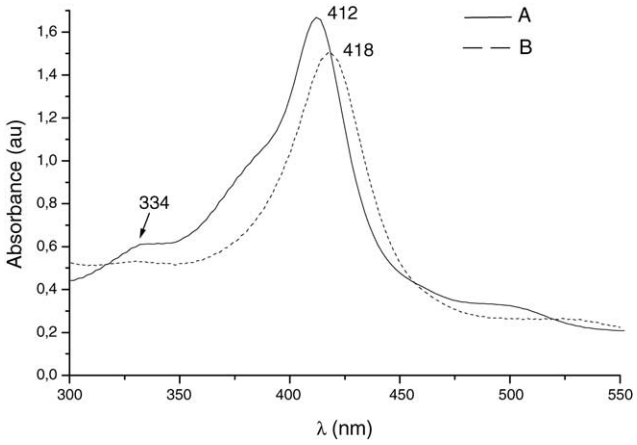

Fig. 3. UV–vis spectra of: (A) a solution of [Fe(TF4TMAPP)]$(PF_6)_5$ 3.8×10^{-4} mol l^{-1} in ACN; (B) after addition of 5.5×10^{-6} mol of (3-mercapto-propyl)-methyldimethoxysilane.

FeP in solution when it is not coordinated with the –SH group (Fig. 4B), indicating a less coordinated Fe(III)-SH system in this case. On the other hand, the spectra of the solid catalysts [Fe{T(4-*N*-MePy)P}]-SiSH and [Fe{T(2-*N*-MePy)P}]-SiSH (Fig. 4A) do not display the band at 334 nm, a pattern that is similar to that of the fully coordinated [Fe(TF4TMAPP)]-SH (Fig. 3B).

The FeP loadings were quantified by measuring the amount of unloaded FeP in the solvent washings by UV–vis spectroscopy (Table 1). As already mentioned [22], systems where ionic binding is favoured, as is the case of $[Fe\{T(2\text{-}N\text{-}MePy)P\}]^{5+}$ and $[Fe\{T(4\text{-}N\text{-}MePy)P\}]^{5+}$ bound to the anionic support $SiSO_3^-$, leads to the highest FeP loadings, and very low catalyst leaching from the support occurs throughout the reaction. Interestingly, the complex $[Fe\{T(2\text{-}N\text{-}MePy)P\}]^{5+}$ bound to the solid support SiSH also led to high catalyst loading, and this can be explained by the fact that, besides the coordination of the sulphur from the support SiSH to iron(III) there probably also is a strong contribution

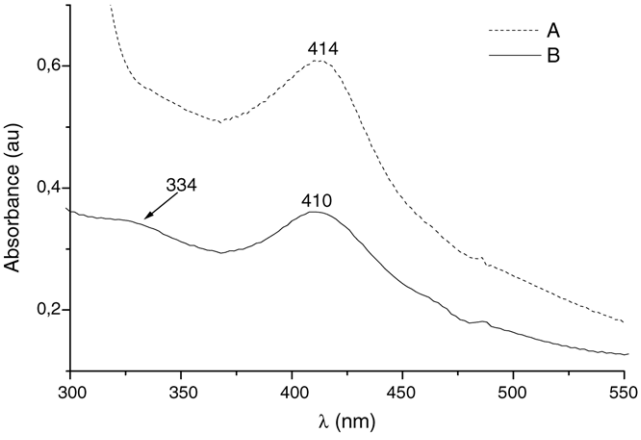

Fig. 4. UV–vis spectra of: (A) a solid suspension of [Fe(TF4TMAPP)]-SiSH in CCl_4; (B) a solid suspension of [Fe{T(2-*N*-MePy)P}]-SiSH in CCl_4.

Table 1
Amount of iron porphyrin bound to the solid supports

Support	FeP	Solvent used in the Soxhlet extractor	Loading (%)
SiSH	$[Fe(TF4TMAPP)]^{5+}$	ACN	97
SiO_2	$[Fe(TF4TMAPP)]^{5+}$	ACN	98
IPG	$[Fe\{T(2\text{-}N\text{-}MePy)P\}]^{5+}$	MeOH	92
$SiSO_3^-$	$[Fe\{T(2\text{-}N\text{-}MePy)P\}]^{5+}$	MeOH	99
SiSH	$[Fe\{T(2\text{-}N\text{-}MePy)P\}]^{5+}$	MeOH	99
SiO_2	$[Fe\{T(2\text{-}N\text{-}MePy)P\}]^{5+}$	MeOH	90
IPG	$[Fe\{T(4\text{-}N\text{-}MePy)P\}]^{5+}$	MeOH	92
$SiSO_3^-$	$[Fe\{T(4\text{-}N\text{-}MePy)P\}]^{5+}$	MeOH	99
SiSH	$[Fe\{T(4\text{-}N\text{-}MePy)P\}]^{5+}$	ACN	100
SiO_2	$[Fe\{T(4\text{-}N\text{-}MePy)P\}]^{5+}$	ACN	99

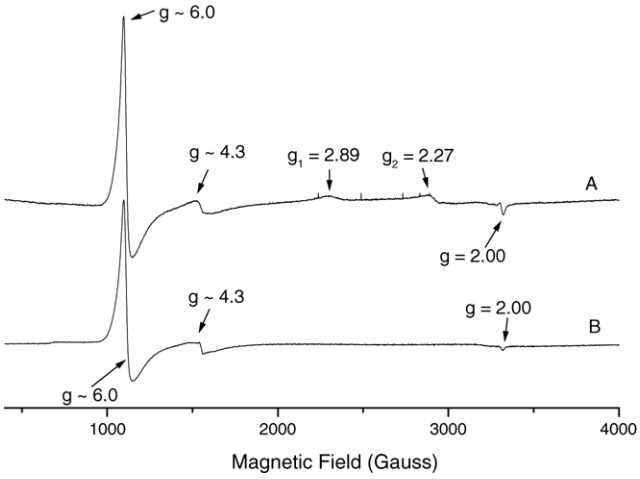

Fig. 5. EPR spectra of: (A) entrapped Im-[FeTFPP]ES and (B) supported [Fe{T(2-*N*-MePy)P}]-IPG.

from the electrostatic interaction between the metalloporpyrin and silanol groups from the support.

The lowest loading was obtained for FeP-IPG, where coordination depends on iron binding to nitrogen.

Analysis of the FePs immobilised on the different solid supports by EPR spectroscopy was also performed. This study provided information on the spin and oxidation states of the central iron present in the anchored FePs, that all the samples contain high-spin iron(III) (signals in $g_\perp \sim 6$ and $g_\parallel \sim 2$), suggesting that the FeP complexes are mono-coordinated to the support in all cases. A typical spectrum of an anchored FeP is shown in Fig. 5B. We also observed a signal in $g = 4.3$, for all the studied systems, which is consistent with a distorted structure for the iron porphyrin.

3.2. Preparation and characterisation of entrapped iron porphyrins (FePES)

Encapsulated iron porphyrins were prepared by the addition of a known quantity of FeP to a silica sol. After drying, the mass of FeP per final mass of material (loading) was determined through repetitive washing of the attained material with several solvents, as earlier described in Section 2. The amount of leached FeP in the combined washings was measured by UV–vis.

Studies of encapsulated FeP (FePES) in the silica matrix have demonstrated that the structure and morphology of the xerogel depend on the porphyrin and on the conditions used during the sol–gel preparation process [24]. Therefore, the best conditions for FeP entrapment were identified. The material obtained after the washings exhibited a brown colour, indicating that the incorporation of FeP really occurred, since the silica matrix without any entrapped molecule presents a white colour [29].

The FeP loading (Table 2) into 4-phIm-[FeTF4TMAPP]ES was lower than the FeP loading of the FePES systems prepared with other FePs. A higher FeP loading was observed in the case of the encapsulated Im-[FeTFPP]ES; if compared to 4-phIm-[[FeTF4TMAPP]ES, where 4-phIm was used as template.

UV–vis studies of FeP samples lead to the same spectrum pattern of the parent iron porphyrins in solution (Table 2) [30], indicating that the structure of the FeP was retained throughout the sol–gel process. The spectra of the xerogels have resolved Soret peaks, but the α and β bands cannot be assigned due to the broadening caused by the silica.

The EPR spectra of the encapsulated FePs displayed high spin Fe^{III} signals in $g_\perp \sim 6.0$ and $g_\parallel \sim 2.0$, and a signal in $g = 4.3$, in all cases, which is consistent with a rhombic structure for the iron porphyrin. The complex Im-[FeTFPP]ES presented signals in $g_1 = 2.89$, $g_2 = 2.27$

Table 2
Properties of the prepared materials: porphyrin loading, UV–vis, EPR and surface area

Catalyst	Loading (μ mol/g ± 1)	UV–vis (nm)	EPR (±0.005)	Surface area (m^2/g ± 10)
$[FeTFPP]^+$	–	412	Fe^{III}(5/2): ~6.0, 2.0	–
Im-[Fe(TFPP)]ES	11.1	413	Fe^{III}(5/2): 6.0, 4.3, 2.0; Fe^{III}(1/2): 2.89, 2.27	14
$[Fe(TF4TMAPP)]^{5+}$ (ACN)	–	408	–	–
4-phIm-[Fe(TF4TMAPP)]ES	1.7	409	Fe^{III}(5/2): ~6.0	633
$[Fe\{T(2\text{-}N\text{-}MePy)P\}]^{5+}$	–	410	Fe^{III}(5/2): ~6, 4.3, 2	–
4-phIm-[Fe{T(2-*N*-MePy)P}]ES	4.3	416	Fe^{III}(5/2): ~6, 4.3, 2	649
$[Fe\{T(4\text{-}N\text{-}MePy)P\}]^{5+}$	–	412	Fe^{III}(5/2): ~6, 4.3, 2	–
4-phIm-[Fe{T(4-*N*-MePy)P}]ES	3.1	416	Fe^{III}(5/2): ~6, 4.3, 2	620

UV–vis spectra were recorded with the solid catalyst in a suspension in CCl_4. The EPR spectra were recorded after adding 0.030–0.050 g of the dry material to an EPR quartz tube.

Table 3
Oxidation of (*Z*)-cyclooctene and cyclohexane by PhIO or H_2O_2, catalysed by encapsulated iron porphyrins and supported iron porphyrind

Sl. no.	Catalyst	Cyclohexane yield (%) PhIO[a] (±5%)		Cyclooctene oxide yield (%)	
		ol	one	PhIO[a] (±5%)	H_2O_2[b] (±5%)
1	[Fe{TFPP}]$^+$	60	3	98	65
2	Im-[Fe{TFPP}]ES	35	3	87	48
3	[Fe(TFPP)]-IPG	64	0	–	–
4	[Fe{TF4TMAPP}]$^{5+}$ (ACN)	33	6	100	75
5	4-phIm-[Fe{TF4TMAPP}]ES	3	0	73	5
6	[Fe(TF4TMAPP)]-SiSH	40	0	84	80
7	[Fe(TF4TMAPP)]-SiO_2	52	5	95	86
8	Fe[T(4-*N*-MePy)P]$^{5+}$ (MeOH)	7	0	50	37
9	4-phIm–[Fe{T(4-*N*-MePy)P}]ES	0[c] (4)	0	29[c] (60)	31
10	[Fe{T(4-*N*-MePy)P}]-SiSH	5	0	100	44
11	[Fe{T(4-*N*-MePy)P}]-SiO_2	20	0	100	54
12	[Fe{T(4-*N*-MePy)P}]-IPG	7	0	65	35
13	[Fe{T(4-*N*-MePy)P}]-$SiSO_3$	2	0	56	41
14	Fe[T(2-*N*-MePy)P]$^{5+}$ (MeOH)	3	0	54	44
15	4-phIm-[Fe{T(2-*N*-MePy)P}]ES	0[c] (2)	0	28[c] (50)	29[c] (26)
16	[Fe{T(2-*N*-MePy)P}]-SiSH	6	0	100	56
17	[Fe{T(2-*N*-MePy)P}]-SiO_2	19	3	100	66
18	[Fe{T(2-*N*-MePy)P}]-IPG	3	0	58	33
19	[Fe{T(2-*N*-MePy)P}]-$SiSO_3$	10	0	61	69

[a] $T = 25\,^{\circ}C$, magnetic stirring, solvent: DCE, cyclooctene/PhIO/catalyst molar ratio = 6000:100:1, [FeP] = 2.5×10^{-7} mol, 200 μl cyclooctene and 800 μl solvent. Yields based on PhIO; [PhIO] = 2.5×10^{-5} mol. Error average 2%, based on the starting PhIO.
[b] $T = 25\,^{\circ}C$, magnetic stirring, solvent: DCM:ACN (1:1), cyclohexane/H_2O_2/catalyst molar ratio = 6000:40:1, [FeP] = 2.5×10^{-7} mol, 200 μl cyclohexane and 800 μl solvent. Yields based on H_2O_2; [H_2O_2] = 1.0×10^{-5} mol. Error average 2%, based on the starting H_2O_2.
[c] After 6 month.

and g_3 not determined. A typical spectrum is shown in Fig. 5A [31]. The exception to this generalisation is 4-phIm-[FeTF4TMAPP]ES, which does present only the high spin Fe^{III} signal in $g = 6$. The UV–vis spectra show the presence of the Fe^{II} species in this catalyst (Table 2).

Each material surface area was determined by the nitrogen adsorption–desorption isotherms of previous degassed solids, at 120 °C. Measurements were carried out at liquid nitrogen boiling point, in a volumetric apparatus, using nitrogen as probe. The xerogels specific surface areas were determined from the *t*-plot analysis [32], and pore size distribution was obtained using the BJH method [33]. All the FePES-templates have surface areas lying between 14 and 649 m^2/g.

3.3. Homogeneous versus heterogeneous systems

For homogeneous systems a good performance of the more resistant fluorosubstituted FeP is normally expected, as in entries 1 and 4 (Table 3). However, iron porphyrins that do not bear electronwithdrawing substituents in the mesophenyl rings may undergo self-oxidative destruction (entryes 8 and 14, Table 3). Besides that, solvents like MeOH and ACN may be oxidised by the active specie $Fe^{IV}(O)P^{\bullet+}$, competing with the substrate and thus decreasing product yields. In the case of cyclohexane hydroxylation, such factors lead to low cyclohexane yields, as is the case of reactions 8 and 14, carried out in MeOH and using electron-deficient catalyst. However, although reaction 4 was also performed in ACN, a solvent that also competes for the active species $Fe^{IV}(O)P^{\bullet+}$, the cicloehane yields was not so low since the catalyst presents electronwithdrawing substituents that stabilise the active species. As for (*Z*)-cyclooctene epoxidation, the cyclooctene oxide yields less affected by these same factors since such substrate is more reactive then cyclohexane.

Thus, a way to prevent catalyst self-oxidative destruction and increase its efficiency is to immobilise it on solid supports. In homogeneous systems, the FePs [Fe{T(4-*N*-MePy)P}]$^{5+}$ and [Fe{T(2-*N*-MePy)P}]$^{5+}$ do not catalyse oxidation reactions in dichloroethane because they are not soluble in this medium, but when supported, [Fe{T(4-*N*-MePy)P}]-SiO_2 (entry 11, Table 3) and [Fe{T(2-*N*-MePy)P}]-SiO_2 (entry 17, Table 3) are particularly more efficient catalysts than their homogeneous analogues (entries 8 and 14, Table 3). This happens because, besides the absence of competitive solvent oxidation with pure DCE, the immobilisation of these FePs renders them more resistant to oxidative self-destruction. This is because these systems consist of a polar hemin in isolated sites, in the same way that the active site of P-450 is a polar protohemin in a hydrophobic pocket, making them good cytochrome P-450 model systems [34].

3.4. Cyclohexane hydroxylation with iodosylbenzene (PhIO)

Selective alkane hydroxylation has been achieved in living organisms by metalloenzymes such as methane monooxygenase and cytochrome P-450 [35]. Product yields and distribution in hydrocarbon oxidations are also largely affected by

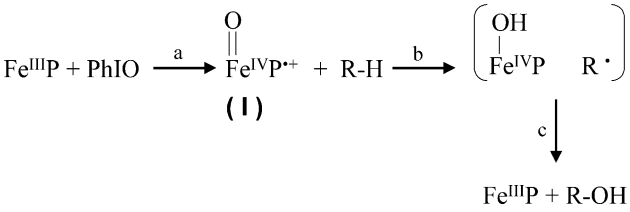

Scheme 1.

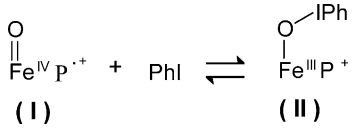

Scheme 2.

the nature of the porphyrin ligands. It is known that for the oxidation of the inert cyclohexane with PhIO, the oxygen rebound mechanism operates [7] (Scheme 1).

In the systems studied in this work, higher yields are obtained with surface supported catalysts, if compared with the encapsulated FePs, as will be explained in detail later. In general, high selectivity torwards cyclohexanol is observed as expected for cytochrome P-450 models.

For the supported [Fe(TF4TMAPP)]$^{5+}$ (Table 3, entries 6 and 7), the presence of electronwithdrawing substituents makes the catalyst more efficient. The active species promotes hydrogen abstraction and renders good cyclohexanol yields.

Comparing all different matrices for each FeP catalyst ([Fe(TF4TMAPP)]$^{5+}$, [Fe{T(4-*N*-MePy)P}]$^{5+}$and [Fe{T(2-*N*-MePy)P}]$^{5+}$) in Table 3, better results are obtained with the FeP–SiO_2 systems, which present a less polar support that does not bear coordinating groups (Table 3, entries 7, 11 and 17). As the substrates are less polar, their access is favoured in these systems, and the products are also easily released from the active site into the solution [36]. In contrast, the more polar systems FeP–$SiSO_3$ (Table 3, entries 13 and 19) lead to low cyclohexanol yields, if compared with the FeP–SiO_2 systems (Table 3, entries 11 and 17).

The solid catalysts [Fe{T(4-*N*-MePy)P}]-SiSH (Table 3, entry 10) and [Fe{T(2-*N*-MePy)P}]-SiSH (Table 3, entry 6) give rise to only 5% and 6% cyclohexanol yields respectively. As aforesaid, these catalytic systems contain the −SH group (section 3.1, Fig. 4B), and there is evidence of SiS-FeP coordination. In the case of [Fe{T(4-*N*-MePy)P}]-IPG and [Fe{T(2-*N*-MePy)P}]-IPG, imidazole also coordinates to the central iron [26], and the yields are low. Although it is known that imidazole coordination favours intermediate I formation (Scheme 1) [37], the coordinations IPG-FeP and SiS-FeP affect the microenvironment of the active site, making the operation of the oxygen rebound mechanism difficult (Scheme 1, pathways b and c), and so hydroxylation becomes less effective. On the other hand, yields are higher for [Fe{T(4-*N*-MePy)P}]-SiO_2 and [Fe{T(2-*N*-MePy)P}]-SiO_2 (Table 3, entries 11 and 17). These better results may be due to the absence of coordinating groups on the support, besides the fact that silica is a less polar support, as discussed before, so the environment favours pathways b and c of the oxygen rebound mechanism.

The solid catalyst [Fe(TF4TMAPP)]-SiSH (Table 3, entry 6) gives rise to 40% cyclohexanol yields. Such high yield can be explained by the presence of electronwithdrawing substituents in the porphyrin ring. Additionally, the absence of SiS-FeP coordination, as observed before (Section 3.1, Fig. 4A), can be considered as favouring this good cyclohexanol yield. Corroborating to the beneficial effect of a less polar support, Fe(TF4TMAPP)]-SiO_2 yielded 52% of cyclohexanol (Table 3, entry 7).

In the case of the encapsulated systems, a high cyclohexanol yield was observed for the electronegatively substituted Im-[FeTFPP]ES complex (35%, Table 3, entry 2). Although EPR spectra gave the evidence of the presence of a small amount of low-spin species (Fig. 5A), the remaining Fe^{III} high-spin species ($g = 6$) were able to promote hydroxylation.

The low yields obtained with the cationic iron porphyrin encapsulated systems (Table 3, entries 5, 9 and 15) can be explained by the nature of the active site environment, which is more polar and rigid, hindering the oxygen rebound mechanism for the hydroxylation of the inert cyclohexane.

Although the complex 4-phIm-[Fe(TF4TMAPP)]ES (Table 3, entry 5) contains electronwithdrawing substituents, cyclohexanol yields was only 3%. In this case, EPR results also (Table 2) indicate the presence of high-spin Fe^{III} signals.

3.5. (Z)-cyclooctene epoxidation with iodosylbenzene (PhIO) or hydrogen peroxide (H_2O_2)

Alkene epoxidation catalysed by FePES and FePs supported on silica and modified silica surface (Fig. 2), by PhIO or H_2O_2 showed that the systems, were able to oxidise (*Z*)-cyclooctene. Better cyclooctene oxide yields were obtained with the FePs supported on surface systems (Table 3).

For the silica supported systems containing electron-deficient FePs [Fe(TF4TMAPP)]-SiSH and [Fe(TF4TMAPP)]-SiO_2 (Table 3, entries 6 and 7), the yields were very good when PhIO was used as oxidant.

The high epoxide yields obtained with the cationic FePs supported on silica [Fe{T(4-*N*-MePy)P}]-SiO_2 and [Fe{T(2-*N*-MePy)P}]-SiO_2 (Table 3, entries 11 and 17) when using PhIO were unexpected, if compared with [Fe{T(4-*N*-MePy)P}]-$SiSO_3$ and [Fe{T(2-*N*-MePy)P}]-$SiSO_3$ (Table 3, entries 13 and 19). Probably, the sulphonate group in the $SiSO_3^-$ support acts as a weakly ligating ligand, and the equilibrium is shifted to intermediate I (Scheme 2), which is responsible for epoxidation [38]. The high yield of 100% obtained in the cases of [Fe{T(4-*N*-MePy)P}]-SiO_2 and [Fe{T(2-*N*-MePy)P}]-SiO_2 (Table 3, entries 11 and 17) can be explained through the operation of an additional intermediate, Fe^{III}-$OIPh^+$. Nam [39] has demonstrated that, in the

reaction of $Fe^{IV}(O)P^{\bullet+}$ (Scheme 2, I) and PhI, there is formation of the Fe^{III}-$OIPh^{+}$ (Scheme 2, II) complex, and this intermediate is able to selectively epoxidise cyclohexene and *cis*-stilbene.

For both systems [Fe{T(4-*N*-MePy)P}]-SiSH and [Fe{T(2-*N*-MePy)P}]-SiSH (Table 3, entries 10 and 16), where the FeP is coordinated to the support, we obtained 100% of cyclooctene oxide yield. Probably, in these systems, intermediate II (Scheme 2) species are also responsible for epoxidation. For [Fe{T(4-*N*-MePy)P}]-IPG and [Fe{T(2-*N*-MePy)P}]-IPG, imidazole from the support coordinated to the FeP, and in this case, intermediate I is favoured, as we have reported before [37].

The results obtained for (*Z*)-cyclooctene epoxidation by H_2O_2 catalysed by heterogeneous systems were high, with the electron-deficient FeP complexes leading to the heterolytic cleavage of the hydroperoxide O–O bond [40].

The supported systems [FeTF4TMAPP]-SiSH and [FeTF4TMAPP]-SiO_2 led to the best results, rendering 80% and 86% cyclooctene oxide yields by using the clean oxidant H_2O_2.

The use of the 2- and 4-*N*-methyl-pyridyl substituted FePs in heterogeneous systems is reported for the first time in this paper in olefin epoxidation by H_2O_2, and the results are comparable with literature data obtained for electron-deficient FePs in homogeneous systems [14,41].

We observed epoxide formation in the case of the encapsulated systems 4-phIm–[Fe{T(4-*N*-MePy)P}]ES and 4-phIm–[Fe{T(2-*N*-MePy)P}]ES (Table 3, entries 9 and 15). However, with more electron-deficient iron porphyrin complexes (Table 3, entry 2), better yields were obtained. In this sense, the exception was 4-phIm-[FeTF4TMAPP]ES (Table 3 entry 5): when H_2O_2 was used, the yield was only 5%. This can be due to the bis-coordination of imidazole to the iron center, which blocks the active site for oxygen binding from the oxidation agent, which is in agrement with the EPR results (Section 3.1, Table 2) [31].

Epoxidation with PhIO significantly increased with 4-phIm–[Fe{T(4-*N*-MePy)P}]ES (Table 3, entry 9) and 4-phIm-[Fe{T(2-*N*-MePy)P}]ES (Table 3, entry 15) after 6 months. Solvent loss probably modified catalyst porosity, intervening in the oxidation process. With the loss of water or methanol, which was the loss washing solvent, intermediate II (Scheme 2) was probably also favoured, as observed in entries 11 and 17 for FePs-supported on silica surface.

4. Conclusion

The present paper has discussed the comparison between different hydrocarbon oxidation catalysts. We have observed that the best systems are the supported FePs, and not the encapsulated FeP systems. In the case of the encapsulated systems, high cyclohexanol and epoxide yields have been observed for the electronegatively substituted Im-[FeTFPP]ES complex. The low yields obtained with the encapsulated cationic iron porphyrin systems can be explained by the nature of the FeP active site environment, which is more polar and rigid, hindering the oxygen rebound mechanism necessary for the hydroxylation of the inert cyclohexane.

For all the cationic iron porphyrins ($[Fe(TF4TMAPP)]^{5+}$, $[Fe\{T(4\text{-}N\text{-}MePy)P\}]^{5+}$ and $[Fe\{T(4\text{-}N\text{-}MePy)P\}]^{5+}$) supported on the simple commercial silica, advantages of FeP binding to the support through electrostatic interaction generally lead to better results using PhIO or H_2O_2 if compared with the two functionalised silica employed in this work. The high epoxidation yields obtained when using PhIO can be explained by the participation of two intermediate species: $Fe^{IV}(O)P^{\bullet+}$ and Fe^{III}-$OIPh^{+}$.

The use of the clean oxidant H_2O_2 in olefin epoxidation in the cases of the 2- and 4-*N*-methyl-pyridyl substituted FePs in heterogeneous systems is reported for the first time in this paper, and the results are comparable with literature data for electron-deficient FePs in homogeneous systems. The best catalyst was obtained by using the iron porphyrin $[Fe(TF4TMAPP)]^{5+}$ and the supports SiSH and SiO_2, rendering 80% and 86% epoxide yields with H_2O_2, respectively.

Acknowledgements

This work was supported by CAPES, CNPq and FAPESP. We are grateful to Prof. Dr. Maurício Rosolen and his group for BET analyses.

References

[1] K.S. Suslick, in: K.M. Kadish, K.M. Smith, R. Guilard (Eds.), The Porphyrin Handbook, vol. 4, Academic Press, New York, 2000, p. 41 (Chapter 28).
[2] B. Meunier, in: B. Meunier (Ed.), Biomimetic Oxidations Catalyzed by Transition Metal Complexes, Imperial College Press, London, 2000, p. 171 (Chapter 4).
[3] T.C. Bruice, Acc. Chem. Res. 24 (1991) 243.
[4] B. Meunier, A. Robert, G. Prativiel, J. Bernadou, in: K.M. Kadish, K.M. Smith, R. Guilard (Eds.), The Porphyrin Handbook, vol.4, Academic Press, New York, 2000, p. 119 (Chapter 31).
[5] W. Nam, S.Y. Oh, Y.J. Sun, J. Kim, W.K. Kim, S.K. Woo, W. Shin, J. Org. Chem. 68 (2003) 7903.
[6] J.R. Lindsay-Smith, in: R.A. Sheldon (Ed.), Metalloporphyrins in Catalytic Oxidations, Kluwer Academic Publishers, Amsterdam, 1994, p. 325 (Chapter 11).
[7] J.T. Groves, Y.Z. Han, in: Ortiz de Montellano (Ed.), Cytocrome P-450: Structure, Mechanism and Biochemistry, 2nd ed., Plenum Publishing, New York, 1995.
[8] D. Mansuy, Coord. Chem. Rev. 125 (1993) 129.
[9] C.K. Chang, F. Ebina, J. Chem. Soc., Chem. Commun. (1981) 778.
[10] T.G. Traylor, S. Tsuchiya, Y.S. Byun, C. Kim, J. Am. Chem. Soc. 115 (1993) 2775.
[11] A.W. Van der Made, J.W.H. Smeets, R.J.M. Nolte, W. Drenth, J. Chem. Soc., Chem. Commun. (1983) 1204.
[12] C.M.C. Prado-Manso, E.A. Vidoto, F.S. Vinhado, H.C. Sacco, K.J. Ciuffi, P.R. Martins, A.G. Ferreira, J.R. Lindsay-Smith, O.R. Nascimento, Y. Iamamoto, J. Mol. Catal. A: Chem. 150 (1999) 251.

[13] F.S. Vinhado, P.R. Martins, A.P. Masson, D.G. Abreu, E.A. Vidoto, O.R. Nascimento, Y. Iamamoto, J. Mol. Catal. A: Chem. 188 (2002) 141.
[14] E.A. Vidoto, M.S.M. Moreira, F.S. Vinhado, K.J. Ciuffi, O.R. Nascimento, Y. Iamamoto, J. Non-Cryst. Solids 304 (2002) 151.
[15] W. Nam, Y.M. Goh, Y.J. Lee, M.H. Lim, C. Kim, Inorg. Chem. 38 (1999) 3238.
[16] J.G. Sharefkin, H. Saltzman, Org. Synth. 5 (1963) 658.
[17] J.S. Lindsey, I.C. Schreiman, H.C. Hsu, P.C. Kearney, A.M. Marguerettaz, J. Org. Chem. 52 (1987) 827.
[18] K.J. Ciuffi, H.C. Sacco, J.C. Biazzotto, E.A. Vidoto, O.R. Nascimento, C.A.P. Leite, O.A. Serra, Y. Iamamoto, J. Non-Cryst. Solids 273 (2000) 100.
[19] E.R. Birnbaum, J.A. Hodge, M.W. Grinstaff, W.P. Schaefer, L. Henling, J.A. Labinger, J.E. Bercaw, H.B. Gray, Inorg. Chem. 34 (1995) 3625.
[20] K.M. Kadish, R. Somg, A. Robert, J. Bernaudou, Inorg. Chim. Acta 272 (1998) 228.
[21] R. Kachadourian, I. Batinié-Haberle, I. Fridovich, Inorg. Chem. 38 (1999) 391.
[22] F.S. Vinhado, C.M.C. Prado-Manso, H.C. Sacco, Y. Iamamoto, J. Mol. Catal. A: Chem. 174 (2001) 279.
[23] O. Leal, D.L. Anderson, R.C. Bowman, F. Basolo, R.L. Burwell, J. Am. Chem. Soc. 97 (1975) 5125.
[24] H.C. Sacco, K.J. Ciuffi, E.A. Vidoto, J.C. Biazzotto, C.A. Mello, D.C. Oliveira, O.A. Serra, O.R. Nascimento, Y. Iamamoto, J. Non-Cryst. Solids 284 (2001) 174.
[25] S. Brunauer, P.H. Emmett, E. Teller, J. Am. Chem. Soc. 60 (1938) 309.
[26] P.R. Cooke, J.R. Lindsay-Smith, J. Chem. Soc., Perkin Trans. 1 (1994) 1913.
[27] C. Gilmartin, J.R. Lindsay-Smith, J. Chem. Soc., Perkin Trans. 2 (1995) 243.
[28] M.A. Martinez-Lorente, P. Battioni, W. Kleemis, J.F. Bartoli, D. Mansuy, J. Mol. Catal. A: Chem. 113 (1996) 343.
[29] C.J. Brinker, G.W. Scherer, Sol–Gel Science: The Physics Of Chemistry of Sol–Gel Processing, Academic Press, 1993.
[30] K.J. Ciuffi, H.C. Sacco, J.B. Valim, C.M.C.P. Manso, O.A. Serra, O.R. Nascimento, E.A. Vidoto, Y. Iamamoto, J. Non-Cryst. Solids 247 (1999) 146.
[31] Y. Iamamoto, K.J. Ciuffi, H.C. Sacco, C.M.C. Prado, M. Moraes, O.R. Nascimento, J. Mol. Catal. A: Chem. 88 (1994) 167.
[32] C.V. Santilli, S.H. Pulcinelli, Cerâmica 39 (1993) 259.
[33] E.P. Barret, L.G. Joyner, P.P. Halenda, J. Am. Chem. Soc. 73 (1951) 373.
[34] Y. Iamamoto, Y.M. Idemori, S. Nakagaki, J. Mol. Catal. A: Chem. 99 (1995) 187.
[35] F.L. Montanari, L. Casella, , in: R.A. Sheldon (Ed.), Metalloporphyrins in Catalytic Oxidations, Kluwer Academic Publishers, Amsterdam, 1994.
[36] A.J. Appleton, S. Evans, J.R. Lindsay-Smith, J. Chem. Soc., Perkin Trans. 2 (1995) 281.
[37] Y. Iamamoto, C.M.C. Prado, H.C. Sacco, K.J. Ciuffi, M.D. Assis, A.P.J. Maestrin, A.J.B. Melo, O. Baffa, O.R. Nascimento, J. Mol. Catal. A: Chem. 117 (1997) 259.
[38] W. Nam, S.W. Jin, M.H. Lim, J.Y. Ryu, C. Kim, Inorg. Chem. 41 (2002) 3647.
[39] W. Nam, S.K. Choi, M.H. Lim, J.U. Rohde, I. Kim, J. Kim, C. Kim, L. Que, Angew. Chem. Int. Ed. 42 (2003) 109.
[40] W. Nam, H.J. Han, S.Y. Oh, Y.J. Lee, M.H. Choi, S.Y. Han, C. Kim, S.K. Woo, W. Shin, J. Am. Chem. Soc. 122 (2000) 8677.
[41] W. Nam, H.J. Lee, S.Y. Oh, C. Kim, H.G. Jang, J. Inorg. Biochem. 80 (2000) 219.